Chemical Geology 498 (2018) 139–149

Contents lists available at ScienceDirect

Chemical Geology

journal homepage: www.elsevier.com/locate/chemgeo

Fluid rock interactions on residual mantle peridotites overlain by shallow oceanic limestones: Insights from Wadi Fins, Sultanate of Oman

Juan Carlos de Obeso*, Peter B. Kelemen

Department of Earth and Environmental Sciences, Lamont Doherty Earth Observatory, Columbia University, 61 Route 9W, Palisades, NY 10964, USA

ARTICLE INFO

Editor: Catherine Chauvel

Keywords:
Serpentinization
Carbonation
Water-rock interaction
Geochemical modeling
Oman
Ophiolite

ABSTRACT

In the southeastern Oman Mountains the mantle section of the Samail ophiolite is unconformably capped by large units of Maastrichtian to Eocene limestones deposited in a shallow marine environment after ophiolite emplacement. In the vicinity of the town of Fins, a deep canyon carved by a stream has exposed mantle sections of the ophiolite. This section is composed of altered peridotites with high concentrations of calcium and small enrichments of silica compared to the Samail mantle protolith suggesting that the peridotites reacted with a hydrous fluid derived from interaction of seawater with the overlying sediments composed of limestones with minor amounts of chert. This is further affirmed by average $\delta^{13}C$ ($-0.25‰_{VPDB}$) $\delta^{18}O$ ($-5.53‰_{VPDB}$) and $^{87}Sr/^{86}Sr$ (0.70788) in the carbonate veins, consistent with values in the sediments. Clumped isotope thermometry on calcite veins in peridotite establish that they formed at 25–60 °C. Reaction path modeling of carbonate-quartz derived fluids with peridotite reproduces the observed mineral assemblage composed of carbonate and serpentine with similar Mg# and MgO/SiO$_2$ at high water to rock ratios, with carbon, H_2O and silica added to the rock by the reacting fluid.

1. Introduction

Mantle peridotite, composed mainly of olivine ($(Mg,Fe)_2SiO_4$) and pyroxenes ($(Ca,Mg,Fe)_2Si_2O_6$), is unstable at Earth's surface conditions and reacts with hydrous fluids to form hydrated silicates (serpentinization), carbonates (carbonation) and oxides. These processes have significant geophysical and geochemical implications. The alteration of peridotite to serpentinite results in drastic changes in the rheology of the rocks (e.g. Escartín et al., 1997; Guillot et al., 2015). Serpentinization of seafloor peridotites is a significant sink for several elements including sulfur, carbon, boron and chlorine (Alt et al., 2013; Alt and Shanks, 1998; Barnes and Sharp, 2006; Bonatti et al., 1984; Boschi et al., 2013; Thompson and Melson, 1970). On land, low temperature serpentinization and carbonation are ubiquitous in peridotite massifs (Barnes et al., 1978; Clark and Fontes, 1990; Kelemen et al., 2011; Kelemen and Matter, 2008; Neal and Stanger, 1985; Paukert et al., 2012; Sánchez-Murillo et al., 2014).

Reaction pathways for serpentinization change depending on temperature, pressure, fluid composition, fluid/rock (W/R) ratios, and primary mineralogy of the protolith. Secondary mineralogy for serpentinization reactions at low temperatures (< 200 °C) is characterized by the presence of lizardite and chrysotile ($Mg_2Si_2O_5(OH)_4$) as the main serpentine minerals (Evans et al., 1976; Evans, 2004) while iron preferentially forms Fe-rich brucite ($(Mg,Fe)(OH)_2$) (Klein et al., 2009; Klein et al., 2013; Seyfried et al., 2007). At higher temperatures antigorite ($(Mg,Fe)_{2.93}Si_{2.07}O_{5.18}(OH)_{3.78}$) is the main serpentine mineral (Evans, 2004; Evans et al., 1976) and magnetite (Fe_3O_4) becomes the main sink for iron (Klein et al., 2014). Early stages of serpentinization are characterized by low water fluxes and strongly reducing conditions (e.g. Bach and Klein, 2009; Frost, 1985; Früh-Green et al., 2004; Schwarzenbach et al., 2014). As serpentinization advances, fluid fluxes increase, resulting in more oxidizing conditions. This leads to sharp changes in oxygen fugacity and secondary mineralogy (Schwarzenbach et al., 2012).

The objective of this paper is to provide constraints on the temperature, fluid composition and fluid source during alteration of mantle peridotite in Wadi Fins, Oman. The results have relevance for understanding carbonation and serpentinization of near-surface mantle peridotite during reaction with sediment-derived fluids.

2. Geologic setting

The Samail ophiolite along the northeast coast of Oman is among the largest and best sub-aerially exposed sections of oceanic crust and its underlying mantle in the world (Coleman, 1977; Coleman and Hopson, 1981; Hopson et al., 1981; Lippard et al., 1986; Pallister and

---

* Corresponding author at: 61 Route 9W, Palisades, NY 10964, USA.
E-mail address: deobeso@ldeo.columbia.edu (J.C. de Obeso).

https://doi.org/10.1016/j.chemgeo.2018.09.022
Received 24 January 2018; Received in revised form 27 August 2018; Accepted 13 September 2018

Knight, 1981). It was thrust over adjacent oceanic lithosphere soon after magmatic formation of oceanic crust at a submarine spreading ridge and then onto the margin of the Arabian subcontinent in the late Cretaceous (Boudier et al., 1996; Hacker, 1994; Hacker and Mosenfelder, 1996; Nicolas et al., 2000; Rioux et al., 2012, 2013; Tilton et al., 1981; Warren et al., 2005).

The mantle section of the ophiolite is mainly composed of highly depleted, residual mantle peridotites (mostly harzburgites, e.g. Godard et al., 2000; Hanghøj et al., 2010; Monnier et al., 2006), together with 5 to 15% dunite (Boudier and Coleman, 1981; Braun and Kelemen, 2002; Braun, 2004; Collier, 2012; Kelemen et al., 2000). These peridotites, thrust toward the surface and then exposed by faulting and erosion, are far from equilibrium with water and carbon dioxide. This disequilibrium causes ubiquitous alteration. The alteration ranges from ∼20% serpentinization in "fresh" rock to nearly 100% replacement of the anhydrous silicates and oxides (olivine, pyroxenes, spinel) with hydrous minerals (mostly serpentine, but also brucite or talc), carbonates (magnesite, dolomite, calcite, hydrous Mg carbonates), and Fe-oxides and oxy-hydroxides (magnetite, hematite, goethite). Alteration probably occurred throughout the history of the ophiolite, beginning near the axis of the oceanic spreading ridges where the Samail ophiolite crust formed (e.g., Gregory and Taylor, 1981), followed by "high temperature" alteration in the late Cretaceous near the basal thrust where metasediments were subducted beneath peridotite ∼100 °C, (Falk and Kelemen, 2015; Nasir et al., 2007; Stanger, 1985), and continuing to the present day (Chavagnac et al., 2013; Clark and Fontes, 1990; Kelemen et al., 2011; Kelemen and Matter, 2008; Mervine et al., 2014; Mervine et al., 2015; Monnin et al., 2011; Neal and Stanger, 1985; Streit et al., 2012).

Mantle peridotites of the Samail ophiolite in Oman were exposed by sub-aerial erosion in the late Cretaceous. They are locally capped by Late Cretaceous (Maastrichtian) laterites (Al-Khirbash, 2015; Nolan et al., 1990), and elsewhere by fluvial conglomerates rich in peridotite cobbles. This was followed by a marine transgression, which deposited shallow marine carbonates over a broad region, including the Qahlah, Simsina and Jafnayn formations (Nolan et al., 1990; Wyns et al., 1992a).

Outcrops of altered peridotite occur in Wadi Fins at the bottom of the water-carved canyon (Fig. 1). These peridotites are unconformably overlain by up to 1–1.5 km. of sediment, mostly shallow water limestones, deposited from the Late Cretaceous (Maastrichtian) to the Eocene (e.g. Mann et al., 1990; Racey, 1995; Searle and Graham, 1982; Wyns et al., 1992a). Regionally, the peridotite in Wadi Fins is pervasively serpentinized and crosscut by an extensive network of carbonate and serpentine-carbonate veins.

Clastic dikes (or "Neptunian veins") of fine-grained grey limestone intrude the peridotite, tapering downward and extending ∼10 m down from the unconformity (Fig. 2). The clastic dikes are best exposed on the south wall of the Wadi where they are spaced roughly 2 to 4 m apart. They contain angular clasts of altered peridotite, especially near their tips. Although these dikes are almost certainly coeval with formation of the carbonate veins in the underlying peridotite, they are cut by a network of somewhat younger carbonate veins.

3. Sample processing and analytical methods

Analyzed samples were collected during the 2013 and 2016 field seasons in Wadi Fins, Oman (Fig. 1). Twenty-three peridotite and six limestone sub-samples were chipped using a jaw crusher and powdered using an alumina puck mill. These were used for elemental and mineralogical analysis. Billets of 16 peridotite samples were sent to Spectrum Petrographics (http://www.petrography.com/) for preparation of polished thin sections.

Powdered samples were analyzed by X-Ray diffraction (XRD), X-Ray fluorescence (XRF) and Inductively Coupled Plasma Optical Emission spectroscopy (ICP-OES) to obtain whole rock and mineralogical compositions. XRD analysis were performed using a Rigaku DMAX-Rapid Microdiffraction system at the American Museum of Natural History (AMNH), diffractograms were analyzed using JADE software to identify main minerals. Major element X-Ray Flourescence and loss on ignition (LOI) analyses of the bulk rocks for 16 peridotite samples was performed by XRF at the Washington State University GeoAnalytical lab (https://environment.wsu.edu/facilities/geoanalytical-lab/). The rest of the peridotite samples and the limestone samples were analyzed using an Agilent 720 Axial ICP-OES that was calibrated to natural standards (Table S1) at Lamont Doherty Earth Observatory (LDEO) using lithium metaborate fusion and nitric acid solution. Sample composition and analytical precision are given in Supplementary table S1.

Polished thin sections of 16 samples were analyzed with a standard petrographic microscope for phase identification where possible. Nine of the sixteen were also quantitatively analyzed using a 5-spectrometer Cameca SX-100 microprobe at AMNH using a 10 μm beam diameter with 15 kV accelerating voltage, 10 nA current and 20–30 s peak time to determine major element composition of phases using natural standards. Calibration information is shown in Supplementary table S2.

Carbonates from carbonate-serpentine veins in seven peridotite samples were separated from the matrix and stained with Alizarin Red S following a modified version of Friedman's (1959) protocol to differentiate between calcite and dolomite. Calcite mineral separates were crushed using a mortar and pestle to form a fine powder for clumped

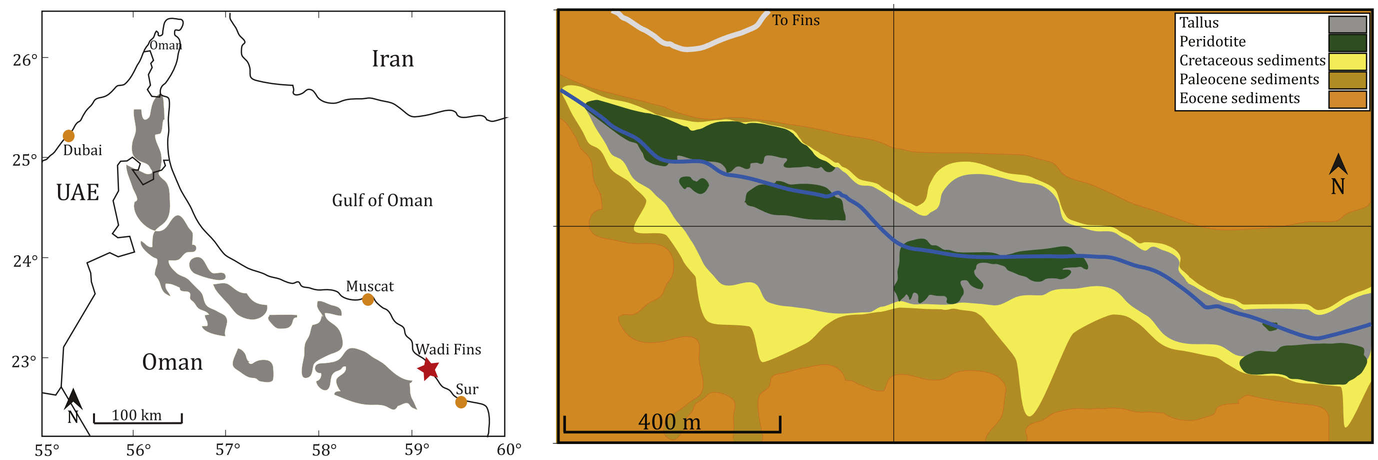

Fig. 1. (Left) Map of the Samail ophiolite after Hanghøj et al. (2010). Red star shows location of Wadi Fins. (Right) Geologic map of Wadi Fins compiled from (Wyns et al., 1992b), Google Earth data and field observations. Map area is between UTM coordinates 2,532,838 to 2,533,636 m N and 721,824 to 722,551 m E in zone 40 Q.

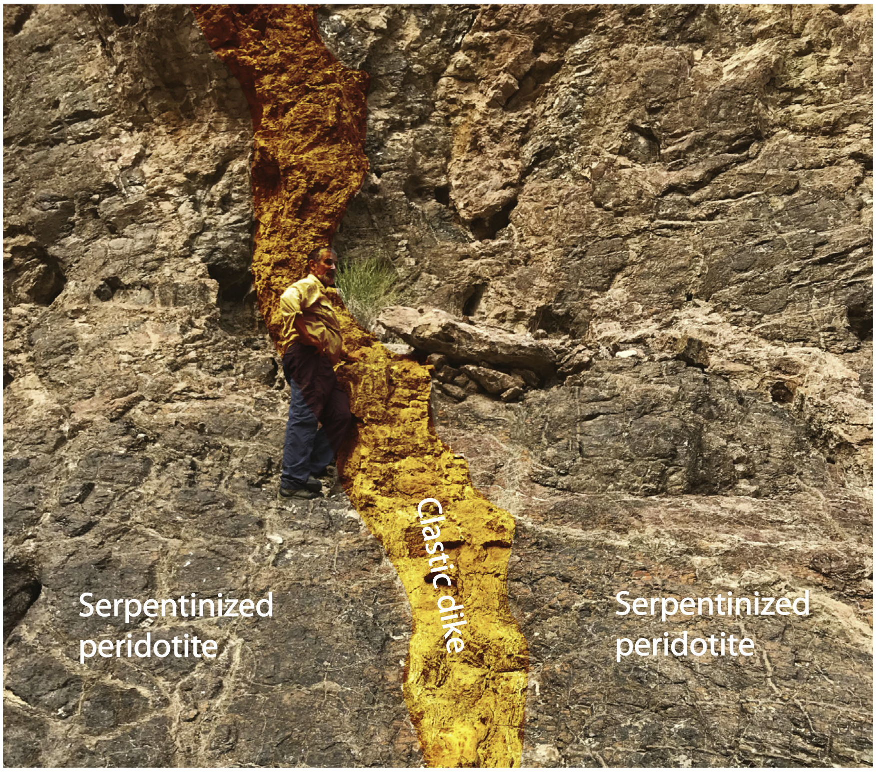

Fig. 2. Clastic dike of limestone (highlighted in yellow) intruding the peridotite in Wadi Fins. A person is shown for scale. (For interpretation of the references to colour in this figure legend, the reader is referred to the web version of this article.)

Table 1

Carbon and oxygen stable isotopes ratios, Δ47, clump temperatures and Sr isotopes ratios for selected carbonates.

Sample	$\delta^{13}C$ ‰ V-PDB	$\delta^{18}O$ ‰ V-PDB	Δ47 ‰	T °C (Ghosh et al., 2006)	T °C (Dennis and Schrag, 2010)	T °C (Bristow et al., 2011)	$^{87}Sr/^{86}Sr$
OM13-1	−0.664 ± 0.020	−5.693 ± 0.006	0.612 ± 0.012	46 ± 3	66 ± 7	56 ± 4	0.707785 ± 0.000010
OM13-11	−0.267 ± 0.032	−5.659 ± 0.194	0.628 ± 0.010	42 ± 2	57 ± 5	50 ± 3	NA
OM13-13	−1.307 ± 0.065	−8.412 ± 0.141	0.716 ± 0.015	22 ± 3	18 ± 6	25 ± 4	0.707895 ± 0.000023
OM13-14A	−0.441 ± 0.033	−8.296 ± 0.144	0.649 ± 0.021	37 ± 5	47 ± 10	44 ± 6	0.707950 ± 0.000012
OM13-15	−0.207 ± 0.018	−3.970 ± 0.143	0.660 ± 0.005	34 ± 1	41 ± 3	40 ± 2	NA
OM13-17A	0.613 ± 0.175	−2.820 ± 0.317	0.658 ± 0.010	34 ± 2	42 ± 4	41 ± 3	NA
OM13-3	0.497 ± 0.092	−3.864 ± 0.095	0.641 ± 0.012	38 ± 3	50 ± 6	46 ± 4	NA

Uncertainties are reported as standard deviation of the replicates of each sample divided by √n-1.

isotope thermometry analysis. Powders were analyzed using a Thermo Finnegan MAT 253 configured to collect masses 44 to 49 isotopologues (cf. Eiler, 2007) at Woods Hole Oceanographic Institution. Analyses, standards and data processing for both sample and standards were carried out following the protocols described by Huntington et al. (2009) and Passey et al. (2010). Three different Δ47 (a measure of isotopologue ^{13}C-^{16}O-^{18}O enrichment compared to a stochastic distribution) temperatures are reported following calibrations by Bristow et al. (2011), Dennis and Schrag (2010), and Ghosh et al. (2006) for comparison (Table 1). All discussion is based on the Bristow et al. Δ47 calibration. Over the analytical run standards 102-GC-AZ01 and NBS19 averaged Δ47 0.728 ± 0.047‰ and 0.436 ± 0.014‰ respectively. These values are either within or close to the range of the average values reported by Dennis et al., 2011 inter-laboratory study, 0.713 ± 0.12‰ (1 S.D.) for 102-GC-AZ01 and 0.392 ± 0.017‰ (1 S.D.) for NBS19. Three of these carbonate separates were dissolved in HNO_3 and analyzed for strontium isotopes ($^{87}Sr/^{86}Sr$) using a ThermoScientific Neptune Plus multi-collector Inductively Coupled Plasma Mass Spectrometer (MC-ICP-MS) in static mode at LDEO, over the run repeat analyses of the NBS-987 Sr-standard averaged a $^{87}Sr/^{86}Sr$ ratio of 0.710252 ± 0.000024, within the NIST SRM value of 0.710248.

4. Results

4.1. Mineralogy and textures in Wadi Fins peridotites

All mantle peridotite samples exhibit high degrees of serpentinization. Relict olivine is rare in thin section but appears in a few samples and even in some diffractograms (OM13-19 and OM13-2). It represents almost 20% of the OM13-19 thin section, making this the least altered sample analyzed for this study. All samples in the matrix have mesh textures typical of serpentine replacing olivine (O'Hanley, 1996; Wicks and Whittaker, 1977). XRD data show that the main serpentine mineral is lizardite with minor occurrences of chrysotile. Relict pyroxenes are present in most thin sections and show various degrees of alteration to serpentine. Olivines and orthopyroxenes have compositions (Supplementary tables S5 and S6) similar to those previously reported in the ophiolite (Hanghøj et al., 2010; Monnier et al., 2006). For samples in which the carbonate content is high enough for XRD identification calcite is the main carbonate phase occurring mostly in veins. Sample OM13-4 is an exception. Here, dolomite occurs in the matrix and is the most abundant carbonate in the sample. Magnesite or brucite were not identified by XRD or microprobe analysis in any sample.

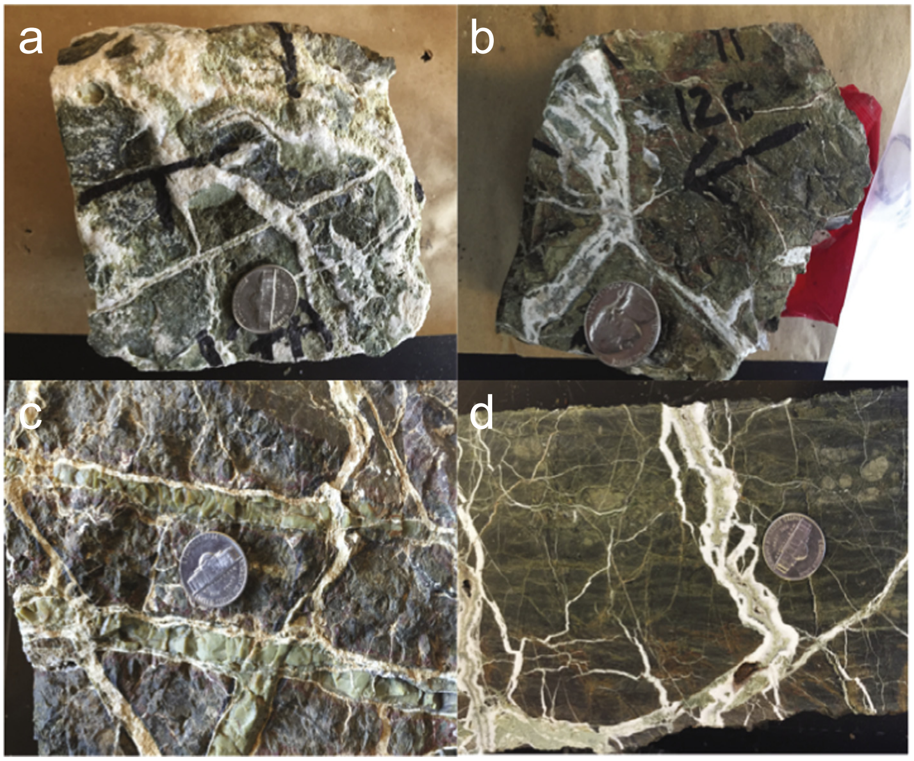

Fig. 3. Examples of serpentine-carbonate veins crosscutting serpentine matrix. (a) OM13-17A, (b) OM13-12C, (c) OM13-15 in which the prominent waxy-green vein below coin is isotropic serpentine and (d) OM13-13. Serpentine in the veins is magnesium rich and contains small magnetite crystals. Coin for scale (D = 2.1 cm). Veins > 0.5 cm are composite serpentine-carbonate. (For interpretation of the references to colour in this figure legend, the reader is referred to the web version of this article.)

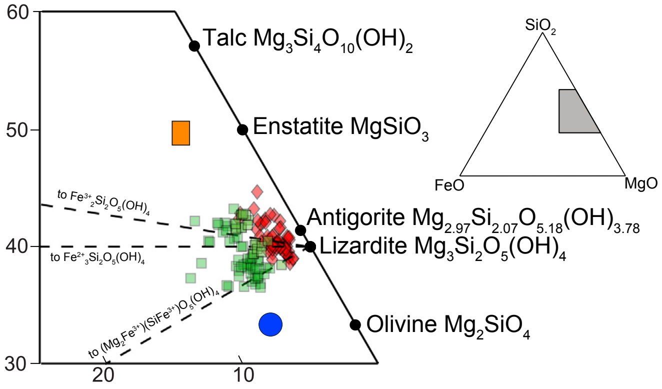

Fig. 4. Projection of electron microprobe analysis of matrix serpentines (green), vein serpentines (red), relict olivines (blue), and pyroxenes (orange) onto a ternary MgO-SiO_2-FeO diagram (molar proportions). All Fe as FeO. (For interpretation of the references to colour in this figure legend, the reader is referred to the web version of this article.)

The outcrops in Wadi Fins contain micron to centimeter scale carbonate veins as well as composite fine-grained serpentine-carbonate veins and rare pure serpentine veins. The alteration phases in the peridotites include matrix serpentine and carbonate-serpentine veins. These phases are evident in the outcrops and hand samples as shown in Fig. 3. While calcite is the most abundant carbonate in the veins dolomite occurs along vein edges in close proximity with serpentine. Serpentine (XRD lizardite) in the mixed serpentine-carbonate veins is in some cases isotropic in cross-polarized light due to its fine-grained nature in the veins. These serpentines usually have low iron contents (X_{Fe} (molar Fe/[Molar Fe + Mg] = 3.8 mol% on average)) compared to matrix serpentines with X_{Fe} = 8.6 mol% on average. Iron oxides occur in the magnesium rich serpentine veins and reach over 50 μm in diameter. Serpentines in the matrix have iron contents similar to or greater than relict olivine and orthopyroxene in samples OM13-2 and OM13-9 (Fig. 4 and Supplementary tables S5 S6, S7 and S8). Iron oxides rarely occur far from veins in the primary serpentine matrix.

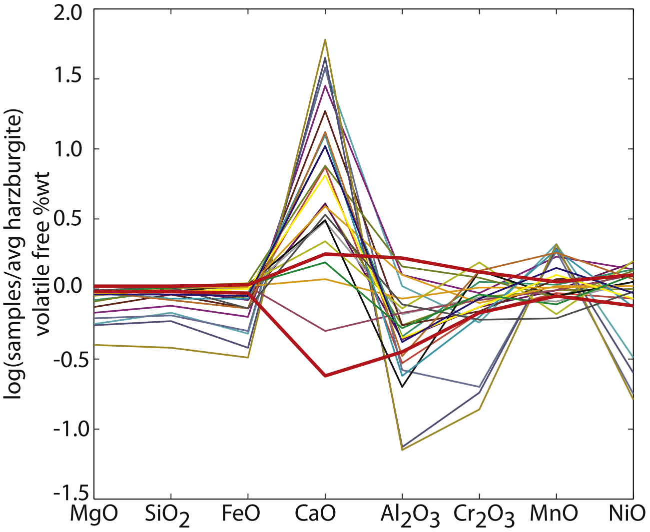

Fig. 5. Major element data compared to average Oman harzburgite. Data are projected from loss-on-ignition (LOI) and the volatile-free composition is ratioed to average Oman harzburgite (Godard et al., 2000; Hanghøj et al., 2010; Monnier et al., 2006) A value of zero (log_{10} of 1) is identical in composition of average Oman harzburgite. Positive values indicate enrichments relative to the protolith, while negative values indicate depletions relative to the protolith. Red thick lines are 2σ deviations from average Oman harzburgite average (Godard et al., 2000; Hanghøj et al., 2010; Monnier et al., 2006). (For interpretation of the references to colour in this figure legend, the reader is referred to the web version of this article.)

4.2. Bulk-rock composition

Almost all Wadi Fins samples show significant enrichment in CaO from the carbonate veins. Larger positive CaO anomalies correlate with larger negative anomalies of most major oxides (MgO, SiO_2, FeO, Al_2O_3,

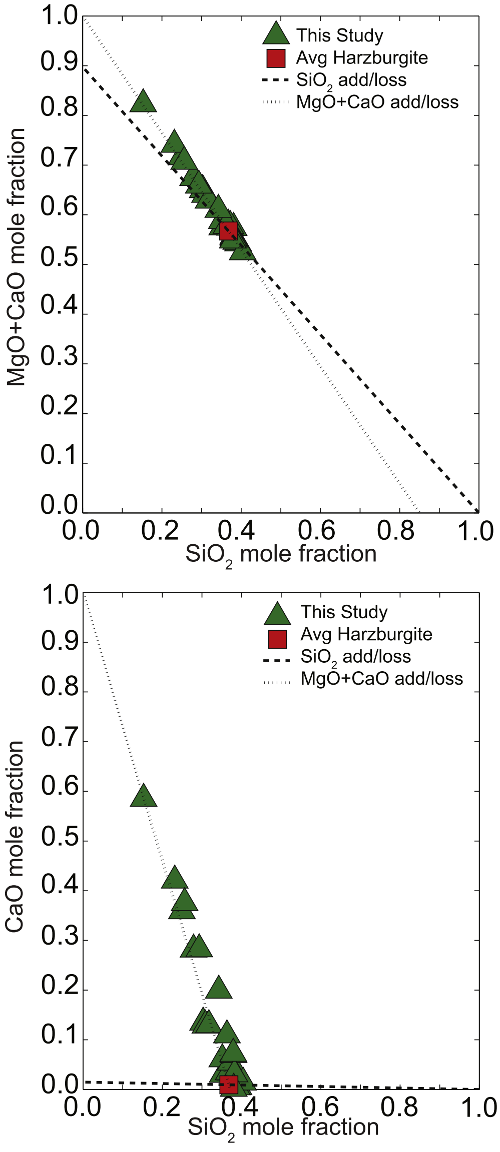

Fig. 6. (Top) Volatile-free molar MgO + CaO versus molar SiO_2. (Bottom) Volatile-free molar CaO versus molar SiO_2. Dashed and dotted grey lines show expected composition if the composition of average Oman harzburgite composition is perturbed only by loss or addition of Mg + Ca or Si. (Average harzburgite from Godard et al., 2000; Hanghøj et al., 2010 and Monnier et al., 2006).

Cr_2O_3). Sample bulk rock compositions are compared to average Oman harzburgite (Godard et al., 2000; Hanghøj et al., 2010; Monnier et al., 2006) in Fig. 5. MnO anomalies correlate with CaO anomalies, because MnO is mainly hosted in carbonate veins (average MnO content in carbonate minerals is 0.6 wt% Supplementary table S9). Calcium contents in bulk rock compositions lie in the expected path of alteration for Oman harzburgite that has modified by addition of calcite (Fig. 6). When projected from calcite the majority of samples are more silica-rich than Oman peridotites (Fig. 7). Bulk rock compositions are reported in Supplementary table S3.

4.3. Carbon, oxygen and Sr isotopes ratios of carbonates veins

Δ47, $\delta^{13}C$, $\delta^{18}O$ and clumped isotope temperatures for 7 samples, and $^{87}Sr/^{86}Sr$ for three of them, are reported in Table 1. Measured Δ47 values of the calcite veins correspond to precipitation temperatures between 25 and 60 °C, consistent with vein formation near the surface.

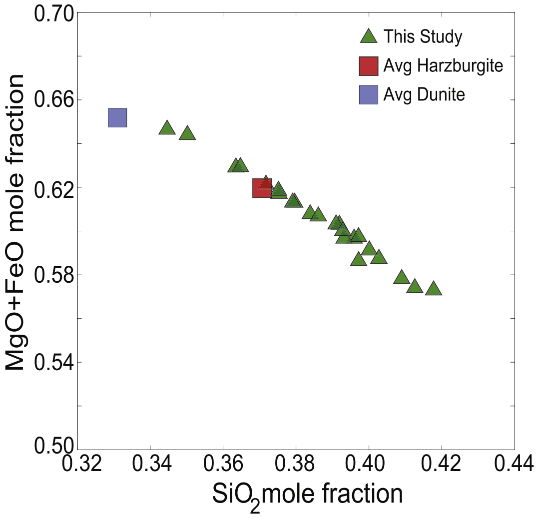

Fig. 7. Volatile-free, calcite-free MgO + FeO vs SiO_2 (projected from CaO + LOI). (Average harzburgite and average dunite from Godard et al., 2000; Hanghøj et al., 2010; Monnier et al., 2006).

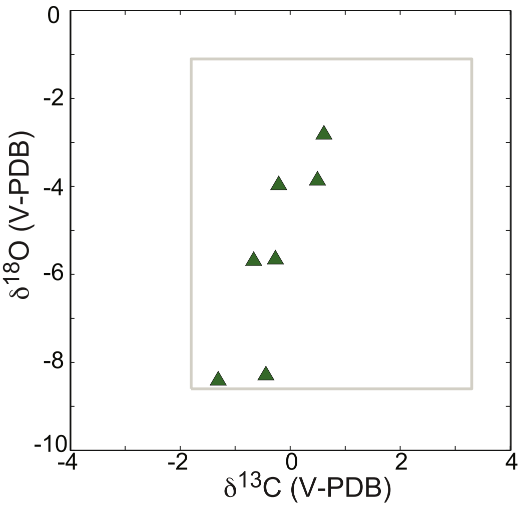

Fig. 8. Stable isotope $\delta^{13}C$ vs. $\delta^{18}O$ of Wadi Fins carbonate veins in green with range observed in the overlying limestone units from Schlüter et al., 2008 in grey. (For interpretation of the references to colour in this figure legend, the reader is referred to the web version of this article.)

Table 2
Initial fluid composition used in the models.

Component	mmol/kg
Na^+	464
Cl^-	546
HCO_3^-	1.56
Ca^{2+}	69.2
Mg^{2+}	29.6
K^+	9.8
SiO_2, aq	0.11
Fe^{2+}	0.0000015
Al^{3+}	0.000037
O_2, aq	0.25
pH	7.8

Ca^{2+}, Mg^{2+} and $HCO3^-$ from Hansen and Wallmann (2003). HCO^{3-} from equilibrium with pCO_2 3× present. All other from Klein et al. (2009).

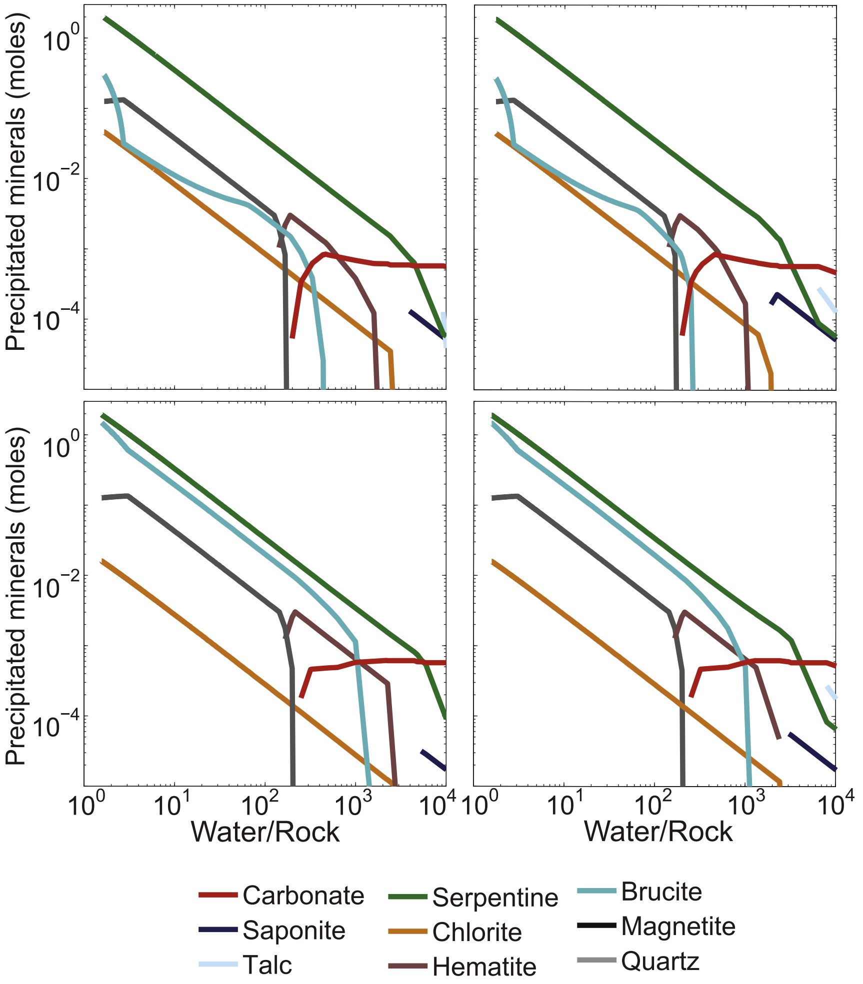

Fig. 9. Mineral reaction products for reaction path models. Top left harzburgite with calcite-saturated fluid; top right harzburgite with calcite-quartz saturated fluid. Bottom left dunite with calcite-saturated-fluid; bottom right dunite with calcite-quartz saturated fluid.

$\delta^{13}C$ and $\delta^{18}O$ in the calcite veins measured are within the range of observed values of Maastrichtian-Eocene sediments in the area (Fig. 8) (Schlüter et al., 2008). $^{87}Sr/^{86}Sr$ ratios of the three measured samples are between 0.70778 and 0.70790, similar to the Cretaceous limestones (Schlüter et al., 2008) and seawater at the Cretaceous-Tertiary (McArthur et al., 2012).

4.4. Bulk rock composition of overlying limestones

The limestones overlying the peridotites are fine-grained. In the unconformity, clastic dikes or “Neptunian veins” of grey limestone intrude the peridotites and contain angular clasts of altered peridotite. Oddly, the clastic dikes appear to root in the unconformity and do not cut the overlying limestone in any outcrop. Above the unconformity, the first few hundred meters of section are mainly composed of limestones. Calcium-rich dolomites occur midsection (~50 m above the unconformity), changing back to limestone at the top of the section. All samples have trace amounts of SiO_2, up to 0.35 wt% with an average of 0.13 wt% for samples within 15 m of the unconformity. Major element compositions of the limestones are reported in Supplementary table S4.

5. Reaction path model

5.1. Model setup

The details of the alteration sequence described above were used to constrain a reaction path model of carbonate-saturated seawater reacting with Oman peridotite using EQ3/6 V 8.0 (Wolery and Jarek, 2003). For all calculations we used the Klein et al. (2009) EQ3/6 thermodynamic database. This database contains equilibrium constants from 0 to 400 °C at 50 MPa, a pressure that we consider within the range expected for the alteration. The model has by three stages. In the first stage, 1 kg of simulated Cretaceous seawater (Table 2) is speciated at 25 °C using EQ3. In the second stage, seawater is heated to 60 °C while reacting with 1 mol of idealized limestone in a closed system. Two idealized limestone compositions were used, one with 100% calcite and a second with 99% calcite and 1% quartz to account to for presence of chert in the Qahlah and Simsina formations (Nolan et al., 1990) In the third stage, the resulting fluid then reacts with rock with the initial composition of average Oman harzburgite (Godard et al., 2000; Hanghøj et al., 2010; Monnier et al., 2006) and dunite (Hanghøj et al., 2010) using EQ6 with special reactant mode in a titration system at 60 °C. The special reactant mode in EQ6 restricts the model to an equilibrium system.

Secondary minerals known to form during serpentinization were allowed to precipitate, forming solid solutions in the third stage of the model (Supplementary table S10). Precipitated minerals in this stage represent the resulting mineralogy produced by the reaction of the input fluid with Oman peridotite. Even though lizardite is the main serpentine mineral in our samples, its thermodynamic properties are not well constrained, so it is not included in the database. Instead, we used chrysotile as the main Mg-serpentine mineral, as its thermodynamic properties are similar to lizardite (Evans, 2004). Results of the third stage are reported using mass ratios of water/rock (W/R = kg

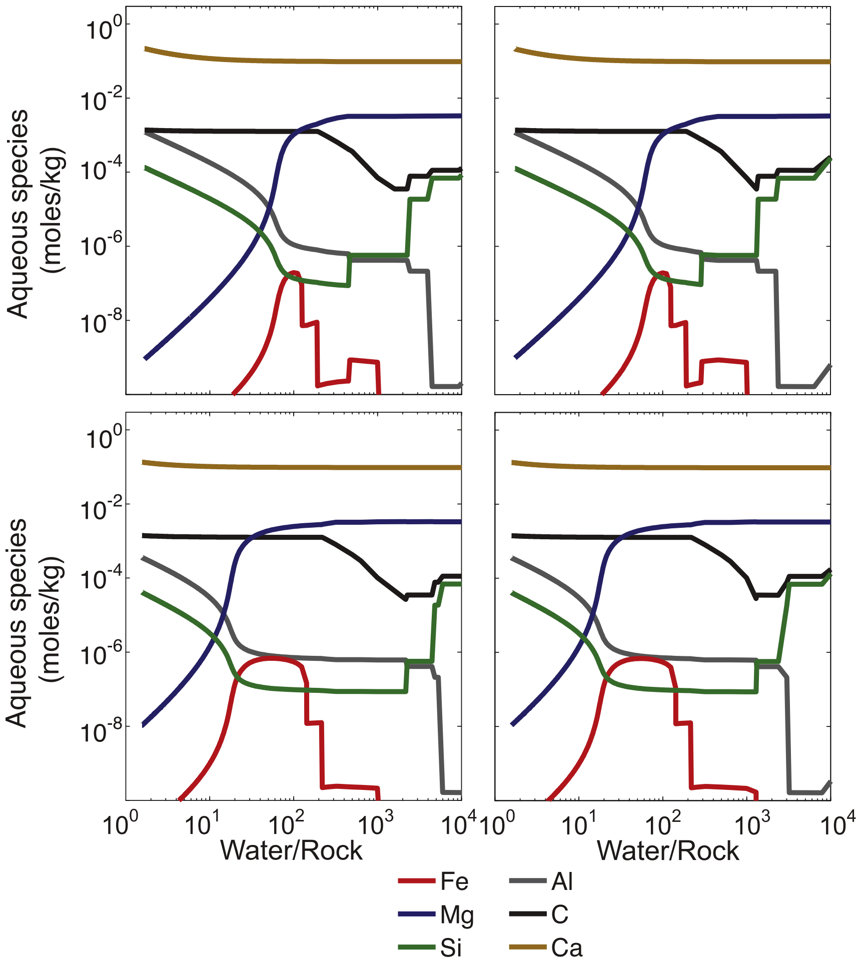

Fig. 10. Fluid chemistry of reaction path models. Top left harzburgite with calcite-saturated fluid; top right harzburgite with calcite-quartz-saturated fluid. Bottom left dunite with calcite-saturated fluid; bottom right dunite with calcite-quartz saturated fluid.

H_2O/kg of rock reacted) following literature convention (e.g. Klein and Garrido, 2011; Klein et al., 2009; Palandri and Reed, 2004).

5.2. Model results

We present the results of four model runs with varying the composition of the peridotite and limestone reactants. These 4 runs are: harzburgite with calcite derived fluid, harzburgite with calcite-quartz derived fluid, dunite with calcite derived fluid and dunite with calcite-quartz derived fluid. Figs. 9–12 summarize the results of these reaction path models.

In all models, mineral appearance and disappearance proceeds in the same order in all models (Fig. 9). Carbonate coexists with serpentine and hematite for $W/R > 100$ and is the dominant phase at $W/R > 5000$. The amount of carbonate minerals is constant along the reaction path for $W/R > 100$. Below W/R of 30 carbonates are unstable and do not appear in the equilibrium assemblage. Below W/R of 5000 serpentine becomes the dominant phase with minor chlorite, brucite and iron oxides (hematite for W/R above 20 and magnetite below). The amount and presence of brucite depends on the peridotite reactant. Both dunite models have brucite occurring at higher W/R ratios than in harzburgites, consistent with higher Mg/Si ratios in dunite compared to harzburgite.

The fluid composition entering the peridotite differs only in the SiO_2(aq) concentration, which is ~5 times higher in the calcite-quartz saturated fluids compared to the calcite saturated fluids. The evolution of the fluid composition evolution is almost identical for the harzburgite and dunite models (Fig. 10). All models show an increase in dissolved Al resulting from a drastic increase in pH (Hitch et al., 1980; May et al., 1979; Wesolowski, 1992). The pH rises to 12 in harzburgite models (Fig. 11) at $W/R < 100$ and up to 11.5 for dunite models at $W/R < 20$. The increase in dissolved Al at high pH in the models is coeval with both an increase in dissolved Si in the fluid, and steep decreases in Mg and Fe. Fe in all models is only soluble at W/R between 20 and 200. All models show abrupt drops in fO_2 at $W/R < 3000$ (Fig. 11) consistent with oxidation of Fe^{2+} in the solid reaction products, and the production of molecular hydrogen from serpentinization of peridotite (Frost, 1985).

Solid mass and volume both increase along the entire reaction path. Mass changes in the models (Fig. 12) are significant with increases over 50% when the system precipitates carbonates at high W/R. Decreasing W/R stabilizes the mass increases to ~16%, mainly from water in the serpentine minerals. Solid volume changes follow a similar path, with significant increases at $W/R > 1000$. Decreasing W/R stabilizes the volume increases to ~40%.

6. Discussion

The presence of peridotite laterite ~12 km from the Wadi Fins location provides evidence that the ophiolite was sub-aerially weathered in a tropical climate (Al-Khirbash et al., 2013; Al-Khirbash, 2015; Alsharhan and Nasir, 1996) after emplacement of the ophiolite onto the Arabian continental margin and erosion of the crustal section in the area. This alteration stage seemingly limited to breccias and fluvial conglomerates along the unconformity in Wadi Fins, was followed by a marine transgression, and deposition of Maastrichtian and younger

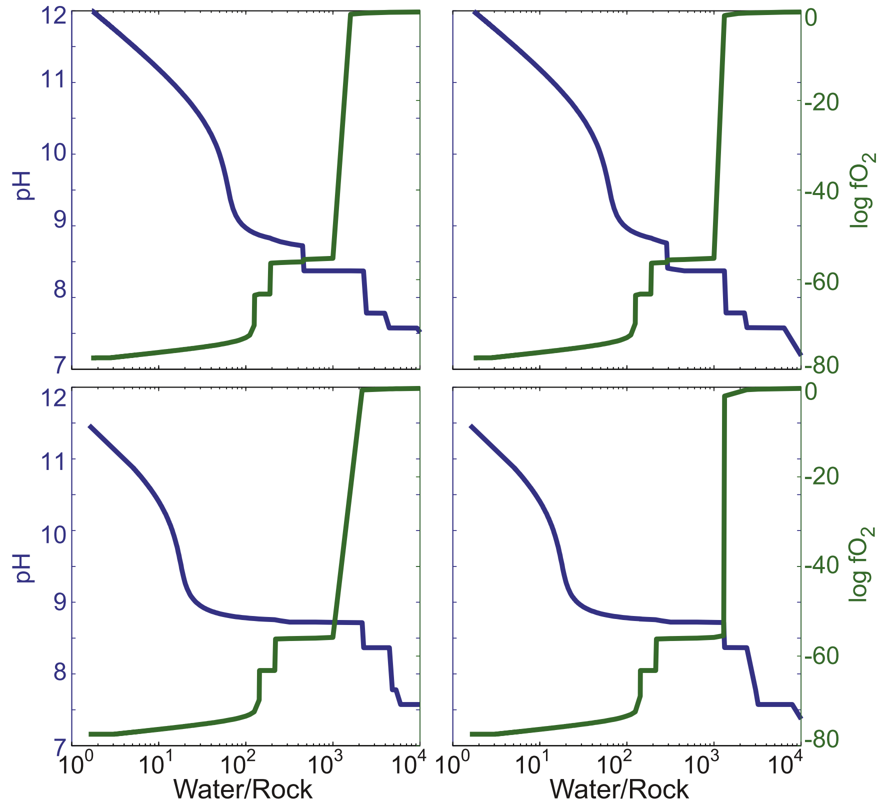

Fig. 11. Reaction path model oxygen fugacity and pH as a function of W/R for reaction path models. Top left harzburgite with calcite-saturated fluid; top right harzburgite with calcite-quartz-saturated fluid. Bottom left dunite with calcite-saturated fluid; bottom right dunite with calcite-quartz-saturated fluid.

sediments – spanning the Cretaceous-Paleogene (K-Pg) boundary – above an unconformity overlying peridotite. $\delta^{13}C$ and $\delta^{18}O$ in the Qahlah, Simsina and Jafnayn limestone formations (Schlüter et al., 2008) are similar to values in our carbonate samples (Fig. 8 and Table 1). $^{87}Sr/^{86}Sr$ ratios are within error of the values reported for the overlying cretaceous limestones (Schlüter et al., 2008) and K-Pg boundary age seawater (McArthur et al., 2012), providing evidence that pore waters in K-Pg age limestone were the source of the fluid that serpentinized and formed veins in the peridotite. Temperatures during alteration, estimated by clumped isotope thermometry, were around 20–60 °C. We infer that the alteration occurred at moderate pressures (300–600 bars) based on limestone unit thickness estimates (Nolan et al., 1990; Racey, 1995; and Wyns et al., 1992a). We also infer that interaction between peridotites and fluids equilibrated with the overlying sediments formed abundant calcite-rich veins and thus resulting in significant CaO enrichments observed in Wadi Fins.

Isochemical serpentinization of olivine-rich rocks requires the formation of a magnesium-rich phase, usually brucite (Evans et al., 1976; Evans, 1977) or magnesite when CO_2-rich fluids are present (Kelemen et al., 2011). We interpret the absence of these minerals in our samples, along with higher SiO_2 contents than average Oman peridotites, as an indication of non-isochemical serpentinization in Wadi Fins.

Wadi Fins peridotites have low Al_2O_3/SiO_2 (< 0.035), similar to other depleted peridotites in Oman (e.g. Godard et al., 2000; Hanghøj et al., 2010; Monnier et al., 2006) with lower MgO/SiO_2 ratios (Fig. 13). The samples follow a trend parallel to the terrestrial geochemical fractionation array (Asimow, 1999; Baker and Beckett, 1999; Jagoutz et al., 1979; Snow and Dick, 1995) at lower MgO/SiO_2 ratios.

MgO/SiO_2 below the geochemical fractionation array is commonly interpreted as a result of alteration processes involving magnesium leaching (Monnier et al., 2006; Snow and Dick, 1995) during alteration. The much lower MgO/SiO_2 in our Wadi Fins samples suggest higher degrees of alteration than in the regionally extensive suite of less altered peridotites studied by Godard et al., 2000; Hanghøj et al., 2010 and Monnier et al., 2006. Extensive leaching of magnesium would result in an appreciable drop in the Mg# (molar Mg)/(Mg + Fe) with decreasing MgO/SiO_2. This is not observed in our samples. On the contrary, several samples have bulk rock Mg# significantly higher (up to 93.3) than most Oman peridotites (Avg Mg# 91, Max Mg# 92 e.g. Godard et al., 2000; Hanghøj et al., 2010; Monnier et al., 2006), and higher than relict primary olivines and pyroxenes in our samples with Mg# ~91. Higher Mg# can either be explained by removal of iron or addition of magnesium. While we infer minor iron mobility, primarily based on observation of iron oxides along veins, we find unlikely that major amounts of iron were preferentially leached to produce higher Mg#. Instead, to explain the low MgO/SiO_2 and variable Mg# in our samples, we prefer to invoke silica addition along with minor amounts of Mg gain or loss. Serpentinization of olivine-rich rocks with addition of silica in the fluid will proceed following the simplified reaction:

$$3\,Mg_2SiO_4 + 2\,SiO_2(aq) + 4\,H_2O = 2\,Mg_3Si_2O_5(OH)_4$$

This reaction forms serpentine without a magnesium rich phase such as brucite or magnesite. Limestones right above the unconformity in Wadi Fins contain small amounts of silica, and chert is present in small quantities in the Qahlah and Simsina formations (Nolan et al., 1990; Schlüter et al., 2008) providing a source of silica to the fluid. Reaction path modeling of calcite-quartz derived fluids with harzburgite and dunite result in MgO/SiO_2 ratios (Fig. 13) that encompass the whole range observed in Wadi Fins at W/R between ~3000 and 1000. In contrast, reaction modeling with fluids that were not initially quartz-saturated does not reproduce the observed compositions of our Wadi Fins samples; the lowest MgO/SiO_2 are 1.02 and 0.90 for dunite and harzburgite respectively at W/R~12,000. W/R as high as those required (~3000 to 1000) to reproduce our sample compositions are predicted to result in significant volume and mass increases. Such solid volume increases represent large strains, which would have caused

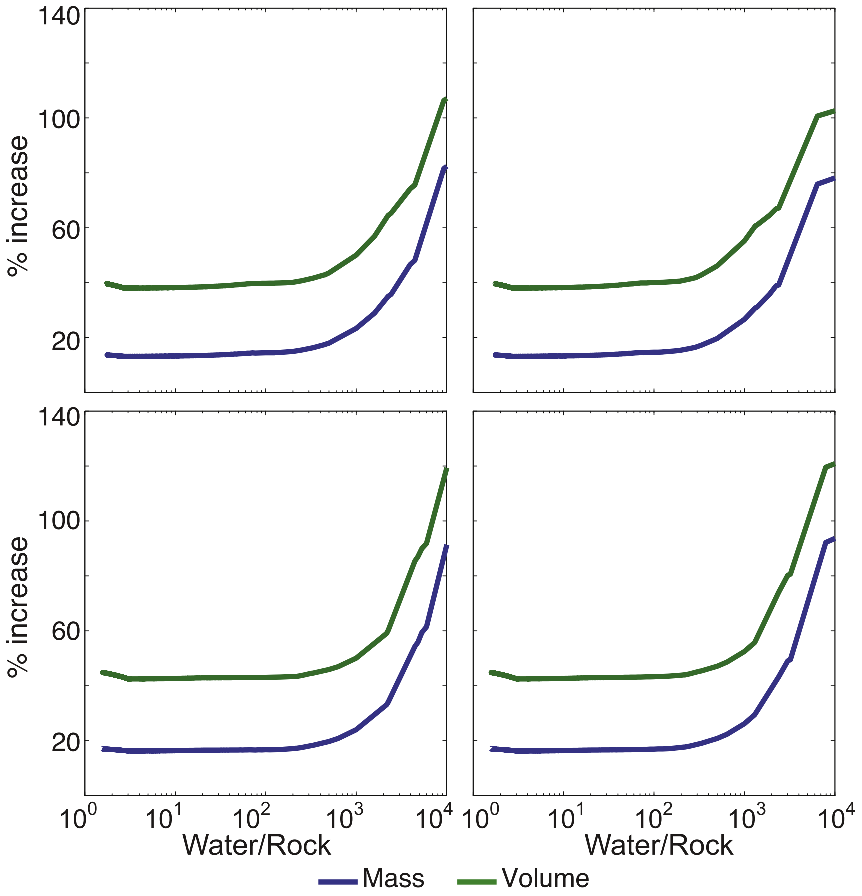

Fig. 12. Reaction path model mass and volume changes as a function of W/R Top left harzburgite with calcite-saturated fluid; top right harzburgite with calcite-quartz saturated fluid. Bottom left dunite with calcite-saturated fluid; bottom right dunite with calcite-quartz-saturated fluid.

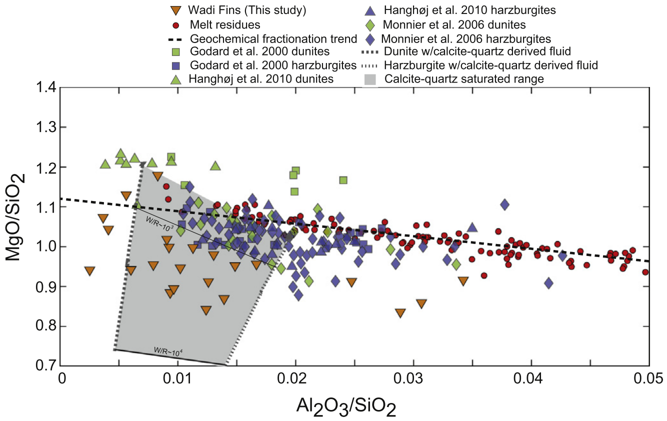

Fig. 13. Whole rock MgO/SiO_2 vs Al_2O_3/SiO_2 for Wadi Fins samples, Oman peridotites (Godard et al., 2000; Hanghøj et al., 2010; Monnier et al., 2006) and peridotite melt residues (Asimow, 1999; Baker and Beckett, 1999). Geochemical fractionation is a linear fit of melt residues (e.g. Jagoutz et al., 1979; Snow and Dick, 1995). Reaction path model results for harzburgite and dunite protoliths are shown for reference (lines). Grey shaded polygon encompass the range of model results for reaction of harzburgite and dunite with calcite-quartz saturated fluids. Tie lines show W/R for the reaction paths.

unrealistically high stresses in an elastic rock matrix. Instead, the resulting elastic stresses must have been relaxed by deformation along fractures due to tectonic stresses and/or reaction-driven cracking (Jamtveit et al., 2008; Kelemen and Hirth, 2012; Macdonald and Fyfe, 1985; Rudge et al., 2010). The opening of existing cracks, and/or formation of new fractures, in turn, may have allowed these large volumes of fluid to react with the rocks.

7. Conclusions

Alteration of the peridotites in Wadi Fins happened in several stages. The first stage probably began near the axis of the oceanic spreading ridge where the Samail ophiolite crust formed (Coleman and Hopson, 1981; Hopson et al., 1981; Lippard et al., 1986) before emplacement. After emplacement some alteration of the uppermost section under tropical weathering conditions is indicated by the presence of the peridotite laterite in outcrops ~12 km to the south of the peridotite outcrops of this study (Al-Khirbash, 2015; Al-Khirbash et al., 2013; Alsharhan and Nasir, 1996; Wyns et al., 1992b). In our field area, breccias and fluvial conglomerates along the unconformity represent this stage of alteration. Sub-aerial weathering was followed by addition of calcium carbonate – mostly in calcite veins – and silica – mostly in serpentine – sourced from the Qahlah and Simsina limestone formations. This alteration took place at 25–60 °C, moderate pressures (< 500 bar) and high W/R.

Reaction path modeling reproduces the mineral assemblage observed in the Wadi Fins samples. At high W/R ratios, carbon and silica are transferred from the fluids into the precipitated minerals. These results reproduce the observed trends in the natural samples, particularly the changes MgO/SiO_2 and Mg#, and mimics the proposed later alteration stage when large volumes of carbonate saturated-seawater circulated through the peridotites, resulting in precipitation of carbonates and serpentine. Results are consistent with previous modeling of peridotite alteration with seawater (e.g. Klein et al., 2009).

This alteration setting provides a window into the modification of peridotites by fluids similar to seawater at low temperatures far from oceanic spreading ridges and provides insights on the behavior of proposed engineered mineral carbonation using seawater as carbon bearing fluid (Kelemen et al., 2011; Kelemen and Matter, 2008). In particular, chemical data and modeling support the inference that solid mass and volume both increase during low temperature alteration of peridotite, leading to large elastic stresses that must be accommodated by deformation along fractures induced by tectonic stresses and/or reaction-driven cracking.

Acknowledgements

We thank everyone at the Sultanate of Oman Public Authority for Mining, especially Dr. Ali Al Rajhi for facilitating our fieldwork in Oman. Editor-in-Chief Catherine Chauvel and two anonymous reviewers are thanked for insightful comments that greatly improved the manuscript. J. Gross, B. Goldoff, G. Harlow, L. Bolge and K. Benedetto are thanked for mentorship in and assistance with laboratory work. We are grateful to F. Klein for providing the database used for reaction-path modeling. We thank W. Guo for opening his lab at WHOI. Many thanks are owed to E. Falk for her help and hospitality during JCdO visit to WHOI. This article benefits from helpful discussions with E. Cooperdock and proof reading from S. Boswell. This work was supported through the Sloan Foundation – Deep Carbon Observatory (Grant 2014-3-01, Kelemen PI), the U.S.-National Science Foundation (NSF-EAR-1516300, Kelemen lead PI). JCdO was partially funded by CONACYT (Fellow 399784).

Appendix A. Supplementary data

Supplementary data to this article can be found online at https://doi.org/10.1016/j.chemgeo.2018.09.022.

References

Al-Khirbash, S., 2015. Genesis and mineralogical classification of Ni-laterites, Oman Mountains. Ore Geol. Rev. 65, 199–212. https://doi.org/10.1016/j.oregeorev.2014.09.022.

Al-Khirbash, S., Semhi, K., Richard, L., Nasir, S., Al-Harthy, A., 2013. Rare earth element mobility during laterization of mafic rocks of the Oman ophiolite. Arab. J. Geosci. 7 (12), 5443–5454. https://doi.org/10.1007/s12517-013-1189-6.

Alsharhan, A.S., Nasir, S., 1996. Sedimentological and geochemical interpretation of a transgressive sequence: the Late Cretaceous Qahlah Formation in the western Oman Mountains, United Arab Emirates. Sediment. Geol. 101 (3–4), 227–242. https://doi.org/10.1016/0037-0738(95)00067-4.

Alt, J.C., Shanks, W.C., 1998. Sulfur in serpentinized oceanic peridotites: Serpentinization processes and microbial sulfate reduction. J. Geophys. Res. 103 (November 2015), 9917. https://doi.org/10.1029/98JB00576.

Alt, J.C., Schwarzenbach, E.M., Früh-Green, G.L., Shanks, W.C., Bernasconi, S.M., Garrido, C.J., ... Marchesi, C., 2013. The role of serpentinites in cycling of carbon and sulfur: Seafloor serpentinization and subduction metamorphism. Lithos 178, 40–54. https://doi.org/10.1016/j.lithos.2012.12.006.

Asimow, P.D., 1999. A model that reconciles major- and trace-element data from abyssal peridotites. Earth Planet. Sci. Lett. 169 (3), 303–319. https://doi.org/10.1016/S0012-821X(99)00084-9.

Bach, W., Klein, F., 2009. The petrology of seafloor rodingites: Insights from geochemical reaction path modeling. Lithos 112 (1–2), 103–117. https://doi.org/10.1016/j.lithos.2008.10.022.

Baker, M.B., Beckett, J.R., 1999. The origin of abyssal peridotites: a reinterpretation of constraints based on primary bulk compositions. Earth Planet. Sci. Lett. 171 (1), 49–61. https://doi.org/10.1016/S0012-821X(99)00130-2.

Barnes, J.D., Sharp, Z., 2006. Achlorine isotope study of DSDP/ODP serpentinized ultramafic rocks: Insights into the serpentinization process. Chem. Geol. 228 (4), 246–265. https://doi.org/10.1016/j.chemgeo.2005.10.011.

Barnes, I., O'Neil, J.R., Trescases, J., 1978. Present day serpentinization in New Caledonia, Oman and Yugoslavia. Geochim. Cosmochim. Acta 42 (1), 144–145. https://doi.org/10.1016/0016-7037(78)90225-9.

Bonatti, E., Lawrence, J.R., Morandi, N., 1984. Serpentinization of oceanic peridotites: temperature dependence of mineralogy and boron content. Earth Planet. Sci. Lett. 70 (1), 88–94. https://doi.org/10.1016/0012-821X(84)90211-5.

Boschi, C., Bonatti, E., Ligi, M., Brunelli, D., Cipriani, A., Dallai, L., ... Bedini, R.M., 2013. Serpentinization of mantle peridotites along an uplifted lithospheric section, Mid Atlantic Ridge at 11° N. Lithos 178, 3–23. https://doi.org/10.1016/j.lithos.2013.06.003.

Boudier, F., Coleman, R.G., 1981. Cross section through the peridotite in the Samail ophiolite, southeastern Oman Mountains. J. Geophys. Res. 86 (B4), 2573. https://doi.org/10.1029/JB086iB04p02573.

Boudier, F., Nicolas, A., Ildefonse, B., 1996. Magma chambers in the Oman ophiolite: fed from the top and the bottom. Earth Planet. Sci. Lett. 144 (1–2), 239–250. https://doi.org/10.1016/0012-821X(96)00167-7.

Braun, M.G., 2004. Petrologic and Microstructural Constraints on Focused Melt Transport in Dunites and Rheology of the Shallow Mantle. WHOI/MIT (Retrieved from). http://oai.dtic.mil/oai/oai?verb=getRecord&metadataPrefix=html&identifier=ADA426948.

Braun, M.G., Kelemen, P.B., 2002. Dunite distribution in the Oman Ophiolite: Implications for melt flux through porous dunite conduits. Geochem. Geophys. Geosyst. 3 (11), 1–21. https://doi.org/10.1029/2001GC000289.

Bristow, T.F., Bonifacie, M., Derkowski, A., Eiler, J.M., Grotzinger, J.P., 2011. A hydrothermal origin for isotopically anomalous cap dolostone cements from south China. Nature 474 (7349), 68–71. https://doi.org/10.1038/nature10096.

Chavagnac, V., Monnin, C., Ceuleneer, G., Boulart, C., Hoareau, G., 2013. Characterization of hyperalkaline fluids produced by low-temperature serpentinization of mantle peridotites in the Oman and Ligurian ophiolites. Geochem. Geophys. Geosyst. 14 (7), 2496–2522. https://doi.org/10.1002/ggge.20147.

Clark, I.D., Fontes, J.-C., 1990. Paleoclimatic reconstruction in northern Oman based on carbonates from hyperalkaline groundwaters. Quat. Res. 33 (3), 320–336. https://doi.org/10.1016/0033-5894(90)90059-T.

Coleman, R.G., 1977. Geologic, Tectonic, and Petrologic Nature of Four Ophiolites. In: Ophiolites: Ancient Oceanic Lithosphere? Springer Berlin Heidelberg, Berlin, Heidelberg, pp. 159–198. https://doi.org/10.1007/978-3-642-66673-5_8.

Coleman, R.G., Hopson, C.A., 1981. Introduction to the Oman Ophiolite special issue. J. Geophys. Res. Solid Earth 86 (B4), 2495–2496. https://doi.org/10.1029/JB086iB04p02495.

Collier, M.L., 2012. Spatial-Statistical Properties of Geochemical Variability as Constraints on Magma Transport and Evolution Processes at Ocean Ridges. Columbia University.

Dennis, K.J., Schrag, D.P., 2010. Clumped isotope thermometry of carbonatites as an indicator of diagenetic alteration. Geochim. Cosmochim. Acta 74 (14), 4110–4122. https://doi.org/10.1016/j.gca.2010.04.005.

Dennis, K.J., Affek, H.P., Passey, B.H., Schrag, D.P., Eiler, J.M., 2011. Defining an absolute reference frame for ‘clumped’ isotope studies of CO$_2$. Geochim. Cosmochim. Acta 75 (22), 7117–7131. https://doi.org/10.1016/j.gca.2011.09.025.

Eiler, J.M., 2007. “Clumped-isotope” geochemistry—the study of naturally-occurring, multiply-substituted isotopologues. Earth Planet. Sci. Lett. 262 (3–4), 309–327. https://doi.org/10.1016/j.epsl.2007.08.020.

Escartín, J., Hirth, G., Evans, B., 1997. Effects of serpentinization on the lithospheric strength and the style of normal faulting at slow-spreading ridges. Earth Planet. Sci. Lett. 151 (3–4), 181–189. https://doi.org/10.1016/S0012-821X(97)81847-X.

Evans, B.W., 1977. Metamorphism of alpine peridotite and serpentinite. Annu. Rev. Earth Planet. Sci. 397–447. https://doi.org/10.1146/annurev.ea.05.050177.002145.

Evans, B.W., 2004. The serpentinite multisystem revisited: chrysotile is metastable. Int. Geol. Rev. 46 (6), 479–506. https://doi.org/10.2747/0020-6814.46.6.479.

Evans, B.W., Johannes, W., Oterdoom, H., Trommsdorff, V., 1976. Stability of chrysotile and antigorite in the serpentinite multisystem. Schweiz. Mineral. Petrogr. Mitt. 56, 79–93.

Falk, E.S., Kelemen, P.B., 2015. Geochemistry and petrology of listvenite in the Samail ophiolite, Sultanate of Oman: complete carbonation of peridotite during ophiolite emplacement. Geochim. Cosmochim. Acta 160, 70–90. https://doi.org/10.1016/j.gca.2015.03.014.

Friedman, G.M., 1959. Identification of carbonate minerals by staining methods. J. Sediment. Res. 29 (1), 87–97. https://doi.org/10.1306/74D70894-2B21-11D7-8648000102C1865D.

Frost, R.B., 1985. On the stability of sulfides, oxides, and native metals in serpentinite. J. Petrol. 26 (June 1983), 31–63. https://doi.org/10.1093/petrology/26.1.31.

Früh-Green, G.L., Connolly, J.A.D., Plas, A., Kelley, D.S., Grobéty, B., 2004. Serpentinization of oceanic peridotites: Implications for geochemical cycles and biological activity. In: AGU Monograph. vol. 144. pp. 119–136. https://doi.org/10.1029/144GM08.

Ghosh, P., Adkins, J., Affek, H.P., Balta, B., Guo, W., Schauble, E.a., ... Eiler, J.M., 2006. 13C−18O bonds in carbonate minerals: a new kind of paleothermometer. Geochim. Cosmochim. Acta 70 (6), 1439–1456. https://doi.org/10.1016/j.gca.2005.11.014.

Godard, M., Jousselin, D., Bodinier, J.-L., 2000. Relationships between geochemistry and structure beneath a palaeo-spreading centre: a study of the mantle section in the Oman ophiolite. Earth Planet. Sci. Lett. 180 (1–2), 133–148. https://doi.org/10.1016/S0012-821X(00)00149-7.

Gregory, R.T., Taylor, H.P., 1981. An oxygen isotope profile in a section of Cretaceous Oceanic Crust, Samail Ophiolite, Oman: evidence for δ^{18}O buffering of the oceans circulation at mid-ocean ridges. J. Geophys. Res. 86 (80), 2737–2755.

Guillot, S., Schwartz, S., Reynard, B., Agard, P., Prigent, C., 2015. Tectonic significance of serpentinites. Tectonophysics 646, 1–19. https://doi.org/10.1016/J.TECTO.2015.01.020.

Hacker, B.R., 1994. rapid emplacement of young oceanic lithosphere: argon geochronology of the Oman ophiolite. Science 265 (5178), 1563–1565. https://doi.org/10.1126/science.265.5178.1563.

Hacker, B.R., Mosenfelder, J.L., 1996. Metamorphism and deformation along the emplacement thrust of the Samail ophiolite, Oman. Earth Planet. Sci. Lett. 144 (3–4), 435–451. https://doi.org/10.1016/S0012-821X(96)00186-0.

Hanghøj, K., Kelemen, P.B., Hassler, D., Godard, M., 2010. Composition and genesis of depleted mantle peridotites from the Wadi Tayin massif, Oman ophiolite; major and trace element geochemistry, and Os isotope and PGE systematics. J. Petrol. 51 (1–2), 201–227. https://doi.org/10.1093/petrology/egp077.

Hansen, K.W., Wallmann, K., 2003. Cretaceous and cenozoic evolution of seawater composition, atmospheric O$_2$ and CO$_2$: A model perspective. Am. J. Sci. 303 (2), 94–148. https://doi.org/10.2475/ajs.303.2.94.

Hitch, B.F., Mesmer, R.E., Baes Jr., C.F., Sweeton, F.H., 1980. The Solubility of (α-Al(OH)$_3$) in 1 Molal NaCl as a Function of pH and Temperature.

Hopson, C.A., Coleman, R.G., Gregory, R.T., Pallister, J.S., Bailey, E.H., 1981. Geologic section through the Samail Ophiolite and associated rocks along a Muscat-Ibra

Transect, southeastern Oman Mountains. J. Geophys. Res. Solid Earth 86 (B4), 2527–2544. https://doi.org/10.1029/JB086iB04p02527.

Huntington, K.W., Eiler, J.M., Affek, H.P., Guo, W., Bonifacie, M., Yeung, L.Y., ... Came, R., 2009. Methods and limitations of "clumped" CO_2 isotope (Delta47) analysis by gas-source isotope ratio mass spectrometry. J. Mass Spectrom. 44 (9), 1318–1329. https://doi.org/10.1002/jms.1614.

Jagoutz, E., Palme, H., Baddenhausen, H., Blum, K., Cendales, M., Dreibus, G., Wanke, H., 1979. The abundances of major, minor and trace elements in the earth's mantle as derived from primitive ultramafic nodules. In: Proceedings of the Lunar and Planetary Science Conference. 10. pp. 2031–2050.

Jamtveit, B., Malthe-Sørenssen, A., Kostenko, O., 2008. Reaction enhanced permeability during retrogressive metamorphism. Earth Planet. Sci. Lett. 267 (3–4), 620–627. https://doi.org/10.1016/j.epsl.2007.12.016.

Kelemen, P.B., Hirth, G., 2012. Reaction-driven cracking during retrograde metamorphism: Olivine hydration and carbonation. Earth Planet. Sci. Lett. 345–348, 81–89. https://doi.org/10.1016/j.epsl.2012.06.018.

Kelemen, P.B., Matter, J.M., 2008. In situ carbonation of peridotite for CO_2 storage. Proc. Natl. Acad. Sci. 105 (45), 17295–17300. https://doi.org/10.1073/pnas.0805794105.

Kelemen, P.B., Braun, M.G., Hirth, G., 2000. Spatial distribution of melt conduits in the mantle beneath oceanic spreading ridges: Observations from the Ingalls and Oman ophiolites. Geochem. Geophys. Geosyst. 1 (7). https://doi.org/10.1029/1999GC000012. (n/a-n/a).

Kelemen, P.B., Matter, J.M., Streit, E.E., Rudge, J.F., Curry, W.B., Blusztajn, J., 2011. Rates and mechanisms of mineral carbonation in peridotite: natural processes and recipes for enhanced, in situ CO_2 capture and storage. Annu. Rev. Earth Planet. Sci. 39 (1), 545–576. https://doi.org/10.1146/annurev-earth-092010-152509.

Klein, F., Garrido, C.J., 2011. Thermodynamic constraints on mineral carbonation of serpentinized peridotite. Lithos 126 (3–4), 147–160. https://doi.org/10.1016/j.lithos.2011.07.020.

Klein, F., Bach, W., Jöns, N., McCollom, T., Moskowitz, B., Berquó, T.S., 2009. Iron partitioning and hydrogen generation during serpentinization of abyssal peridotites from 15°N on the Mid-Atlantic Ridge. Geochim. Cosmochim. Acta 73 (22), 6868–6893. https://doi.org/10.1016/j.gca.2009.08.021.

Klein, F., Bach, W., McCollom, T.M., 2013. Compositional controls on hydrogen generation during serpentinization of ultramafic rocks. Lithos 178, 55–69. https://doi.org/10.1016/j.lithos.2013.03.008.

Klein, F., Bach, W., Humphris, S.E., Kahl, W.-A., Jöns, N., Moskowitz, B., Berquó, T.S., 2014. Magnetite in seafloor serpentinite—some like it hot. Geology 42, 135–138. https://doi.org/10.1130/g35068.1.

Lippard, S.J., Shelton, A.W., Gass, I.G., 1986. The ophiolite of northern Oman. Geol. Soc. Mem. 11 (Retrieved from). http://ci.nii.ac.jp/naid/10014849537/en/.

Macdonald, A.H., Fyfe, W.S., 1985. Rate of serpentinization in seafloor environments. Tectonophysics 116 (1–2), 123–135. https://doi.org/10.1016/0040-1951(85)90225-2.

Mann, A., Hanna, S.S., Nolan, S.C., 1990. The post-Campanian tectonic evolution of the Central Oman Mountains: tertiary extension of the Eastern Arabian Margin. Geol. Soc. Lond., Spec. Publ. 49 (1), 549–563. https://doi.org/10.1144/GSL.SP.1992.049.01.33.

May, H.M., Helmke, P.A., Jackson, M.L., 1979. Gibbsite solubility and thermodynamic properties of hydroxy-aluminum ions in aqueous solution at 25 °C. Geochim. Cosmochim. Acta 43 (6), 861–868. https://doi.org/10.1016/0016-7037(79)90224-2.

McArthur, J.M., Howarth, R.J., Shields, G.A., 2012. Chapter 7 - Strontium Isotope Stratigraphy BT - The Geologic Time Scale. Elsevier, Boston, pp. 127–144. https://doi.org/10.1016/B978-0-444-59425-9.00007-X.

Mervine, E.M., Humphris, S.E., Sims, K.W.W., Kelemen, P.B., Jenkins, W.J., 2014. Carbonation rates of peridotite in the Samail Ophiolite, Sultanate of Oman, constrained through ^{14}C dating and stable isotopes. Geochim. Cosmochim. Acta 126, 371–397. https://doi.org/10.1016/j.gca.2013.11.007.

Mervine, E.M., Sims, K.W.W., Humphris, S.E., Kelemen, P.B., 2015. Applications and limitations of U–Th disequilibria systematics for determining ages of carbonate alteration minerals in peridotite. Chem. Geol. 412, 151–166.

Monnier, C., Girardeau, J., Le Mée, L., Polvé, M., 2006. Along-ridge petrological segmentation of the mantle in the Oman ophiolite. Geochem. Geophys. Geosyst. 7 (11). https://doi.org/10.1029/2006GC001320. (n/a-n/a).

Monnin, C., Chavagnac, V., Ceuleneer, G., Boulart, C., Hoareau, G., 2011. Characterization of hyperalkaline fluids produced by serpentinization of mantle peridotites in Oman and in Liguria (Northern Italy). Mineral. Mag. 75, 1490.

Nasir, S., Al Sayigh, A.R., Al Harthy, A., Al-Khirbash, S., Al-Jaaidi, O., Musllam, A., ... Al-Bu'saidi, S., 2007. Mineralogical and geochemical characterization of listwaenite from the Semail Ophiolite, Oman. Chemie Der Erde – Geochem. 67 (3), 213–228. https://doi.org/10.1016/j.chemer.2005.01.003.

Neal, C., Stanger, G., 1985. Past and present serpentinization of ultramafic rocks: An example from the Semail ophiolite nappe of northern Oman. In: Drewer, J. (Ed.), The Chemistry of Weathering. D. Reidel Publishing Company, Dordrecht, Holland, pp. 249–275.

Nicolas, A., Boudier, F., Ildefonse, B., Ball, E., 2000. Accretion of Oman and United Arab Emirates ophiolite–discussion of a new structural map. Mar. Geophys. Res. 147–179. https://doi.org/10.1023/A:1026769727917.

Nolan, S.C., Skelton, P.W., Clissold, B.P., Smewing, J.D., 1990. Maastrichtian to early Tertiary stratigraphy and palaeogeography of the Central and Northern Oman Mountains. Geol. Soc. Lond., Spec. Publ. 49 (1), 495–519. https://doi.org/10.1144/GSL.SP.1992.049.01.31.

O'Hanley, D.S., 1996. Serpentinites: Records of Tectonic and Petrological History. Oxford University Press, New York and Oxford.

Palandri, J.L., Reed, M.H., 2004. Geochemical models of metasomatism in ultramafic systems: serpentinization, rodingitization, and sea floor carbonate chimney precipitation. Geochim. Cosmochim. Acta 68 (5), 1115–1133. https://doi.org/10.1016/j.gca.2003.08.006.

Pallister, J., Knight, R., 1981. Rare-earth element geochemistry of the Samail Ophiolite near Ibra, Oman. J. Geophys. Res. Solid Earth 86 (B4), 2673. https://doi.org/10.1029/JB086iB04p02673.

Passey, B.H., Levin, N.E., Cerling, T.E., Brown, F.H., Eiler, J.M., 2010. High-temperature environments of human evolution in East Africa based on bond ordering in paleosol carbonates. Proc. Natl. Acad. Sci. U. S. A. 107 (25), 11245–11249. https://doi.org/10.1073/pnas.1001824107.

Paukert, A.N., Matter, J.M., Kelemen, P.B., Shock, E.L., Havig, J.R., 2012. Reaction path modeling of enhanced in situ CO_2 mineralization for carbon sequestration in the peridotite of the Samail Ophiolite, Sultanate of Oman. Chem. Geol. 330–331, 86–100. https://doi.org/10.1016/j.chemgeo.2012.08.013.

Racey, A., 1995. Lithostratigraphy and larger foraminiferal (nummulitid) biostratigraphy of the Tertiary of northern Oman. Micropaleontology 41, 1. https://doi.org/10.2307/1485849.

Rioux, M., Bowring, S., Kelemen, P.B., Gordon, S., Dudás, F., Miller, R., 2012. Rapid crustal accretion and magma assimilation in the Oman-U.A.E. ophiolite: High precision U-Pb zircon geochronology of the gabbroic crust. J. Geophys. Res. 117 (B7), B07201. https://doi.org/10.1029/2012JB009273.

Rioux, M., Bowring, S., Kelemen, P.B., Gordon, S., Miller, R., Dudás, F., 2013. Tectonic development of the Samail ophiolite: High-precision U-Pb zircon geochronology and Sm-Nd isotopic constraints on crustal growth and emplacement. J. Geophys. Res. Solid Earth 118 (5), 2085–2101. https://doi.org/10.1002/jgrb.50139.

Rudge, J.F., Kelemen, P.B., Spiegelman, M., 2010. A simple model of reaction-induced cracking applied to serpentinization and carbonation of peridotite. Earth Planet. Sci. Lett. 291 (1), 215–227. https://doi.org/10.1016/j.epsl.2010.01.016.

Sánchez-Murillo, R., Gazel, E., Schwarzenbach, E.M., Crespo-Medina, M., Schrenk, M.O., Boll, J., Gill, B.C., 2014. Geochemical evidence for active tropical serpentinization in the Santa Elena Ophiolite, Costa Rica: an analog of a humid early Earth? Geochem. Geophys. Geosyst. 15, 1783–1800. https://doi.org/10.1002/2013GC005213.

Schlüter, M., Steuber, T., Parente, M., Mutterlose, J., 2008. Evolution of a Maastrichtian–Paleocene tropical shallow-water carbonate platform (Qalhat, NE Oman). Facies 54 (4), 513–527. https://doi.org/10.1007/s10347-008-0150-8.

Schwarzenbach, E.M., Früh-Green, G.L., Bernasconi, S.M., Alt, J.C., Shanks, W.C., Gaggero, L., Crispini, L., 2012. Sulfur geochemistry of peridotite-hosted hydrothermal systems: comparing the Ligurian ophiolites with oceanic serpentinites. Geochim. Cosmochim. Acta 91, 283–305. https://doi.org/10.1016/j.gca.2012.05.021.

Schwarzenbach, E.M., Gazel, E., Caddick, M.J., 2014. Hydrothermal processes in partially serpentinized peridotites from Costa Rica: evidence from native copper and complex sulfide assemblages. Contrib. Mineral. Petrol. 168. https://doi.org/10.1007/s00410-014-1079-2.

Searle, M.P., Graham, G.M., 1982. "Oman Exotics"—Oceanic carbonate build-ups associated with the early stages of continental rifting. Geology 10 (1), 43. https://doi.org/10.1130/0091-7613(1982)10 < 43:OECBAW > 2.0.CO;2.

Seyfried, W.E., Foustoukos, D.I., Fu, Q., 2007. Redox evolution and mass transfer during serpentinization: an experimental and theoretical study at 200 °C, 500 bar with implications for ultramafic-hosted hydrothermal systems at Mid-Ocean Ridges. Geochim. Cosmochim. Acta 71 (15), 3872–3886. https://doi.org/10.1016/j.gca.2007.05.015.

Snow, J.E., Dick, H.J.B., 1995. Pervasive magnesium loss by marine weathering of peridotite. Geochim. Cosmochim. Acta 59 (20), 4219–4235. https://doi.org/10.1016/0016-7037(95)00239-V.

Stanger, G., 1985. Silicified serpentinite in the Semail nappe of Oman. Lithos 18, 13–22. https://doi.org/10.1016/0024-4937(85)90003-9.

Streit, E.E., Kelemen, P.B., Eiler, J.M., 2012. Coexisting serpentine and quartz from carbonate-bearing serpentinized peridotite in the Samail Ophiolite, Oman. Contrib. Mineral. Petrol. 164 (5), 821–837. https://doi.org/10.1007/s00410-012-0775-z.

Thompson, G., Melson, W.G., 1970. Boron contents of serpentinites and metabasalts in the oceanic crust: Implications for the boron cycle in the oceans. Earth Planet. Sci. Lett. 8 (1), 61–65. https://doi.org/10.1016/0012-821X(70)90100-7.

Tilton, G.R., Hopson, C.A., Wright, J.E., 1981. Uranium-lead isotopic ages of the Samail Ophiolite, Oman, with applications to Tethyan ocean ridge tectonics. J. Geophys. Res. 86 (B4), 2763. https://doi.org/10.1029/JB086iB04p02763.

Warren, C.J., Parrish, R.R., Waters, D.J., Searle, M.P., 2005. Dating the geologic history of Oman's Semail ophiolite: insights from U-Pb geochronology. Contrib. Mineral. Petrol. 150 (4), 403–422. https://doi.org/10.1007/s00410-005-0028-5.

Wesolowski, D.J., 1992. Aluminum speciation and equilibria in aqueous solution: I. The solubility of gibbsite in the system Na-K-Cl-OH-Al(OH)4 from 0 to 100 °C. Geochim. Cosmochim. Acta 56 (3), 1065–1091. https://doi.org/10.1016/0016-7037(92)90047-M.

Wicks, F.J., Whittaker, E., 1977. Serpentine textures and serpentinization. Can. Mineral. 15, 459–488.

Wolery, T.J., Jarek, R.L., 2003. EQ3/6, version 8.0—Software User's Manual. Civilian Radioactive Waste Management System, Management & Operating Contractor. Sandia National Laboratories, Albuquerque, New Mexico.

Wyns, R., Bechennec, F., Le Meteour, J., Roger, J., 1992a. Explanatory Notes to the Geological Map of the Tiwi Quadrangle, Sultanate of Oman. Geoscience Map, Scale 1:100,000, Sheet NF 40-8B. Ministry of Petroleum and Minerals, Directorate General of Minerals, Sultanate of Oman.

Wyns, R., Bechennec, F., Le Meteour, J., Roger, J., 1992b. Geologic Map of Tiwi. Muscat, Oman, Ministry of Petroleum and Minerals, Directorate General of Minerals, Sultanate of Oman. Wallmanna.